Published in final edited form as:
Toxicol Appl Pharmacol. 2008 July 15; 230(2): 235–246.

Arsenite-induced mitotic death involves stress response and is independent of tubulin polymerization

B. Frazier Taylor, **Samuel C. McNeely***, **Heather L. Miller**, and **J. Christopher States**
Department of Pharmacology and Toxicology, Center for Environmental Genomics and Integrative Biology, Center for Genetics and Molecular Medicine, James Graham Brown Cancer Center, University of Louisville, Louisville, KY 40202

Abstract

Arsenite, a known mitotic disruptor, causes cell cycle arrest and cell death at anaphase. The mechanism causing mitotic arrest is highly disputed. We compared arsenite to the spindle poisons nocodazole and paclitaxel. Immunofluorescence analysis of α-tubulin in interphase cells demonstrated that, while nocodazole and paclitaxel disrupt microtubule polymerization through destabilization and hyperpolymerization, respectively, microtubules in arsenite-treated cells remain comparable to untreated cells even at supra-therapeutic concentrations. Immunofluorescence analysis of α-tubulin in mitotic cells showed spindle formation in arsenite- and paclitaxel-treated cells but not in nocodazole-treated cells. Spindle formation in arsenite-treated cells appeared irregular and multi-polar. γ-tubulin staining showed that cells treated with nocodazole and therapeutic concentrations of paclitaxel contained two centrosomes. In contrast, most arsenite-treated mitotic cells contained more than two centrosomes, similar to centrosome abnormalities induced by heat shock. Of the three drugs tested, only arsenite treatment increased expression of the inducible isoform of heat shock protein 70 (HSP70i). HSP70 and HSP90 proteins are intimately involved in centrosome regulation and mitotic spindle formation. HSP90 inhibitor 17-DMAG sensitized cells to arsenite treatment and increased arsenite-induced centrosome abnormalities. Combined treatment of 17-DMAG and arsenite resulted in a supra-additive effect on viability, mitotic arrest, and centrosome abnormalities. Thus, arsenite-induced abnormal centrosome amplification and subsequent mitotic arrest is independent of effects on tubulin polymerization and may be due to specific stresses that are protected against by HSP90 and HSP70.

Introduction

Arsenic trioxide (Trisenox®) is approved by the FDA for treatment of all-trans retinoic acid (ATRA) refractory acute promyelocytic leukemia (APL) (Cohen *et al.*, 2001). Arsenic has history as a chemotherapeutic for leukemia in both traditional Chinese medicine and western medicine from 19th to mid-20th century as well as for treatment of trypanosomiasis and syphilis (Antman, 2001;Waxman and Anderson, 2001). Recent studies have shown that arsenite (administered as As_2O_3) has potential to be effective in hematological malignancies such as newly diagnosed APL, acute myeloid leukemia, myelodysplastic syndromes, multiple

Corresponding author: J. Christopher States, Ph. D., Dept. Pharmacology & Toxicology, University of Louisville, 570 S. Preston St., Suite 221, Louisville, KY 40202, TEL: 502-852-5347, FAX: 502-853-2492, email: jcstates@louisville.edu.
*Current address: Samuel C. McNeely, Ph. D., 408 Z1841, Memorial Sloan-Kettering Cancer Center, 408 East 69th St., New York, NY 10021

myeloma (MM) and chronic myelogenous leukemia either as a single agent or in combined therapy (Amadori *et al.*, 2005). *In vitro*, arsenite induces apoptosis in numerous leukemia and solid tumor cell lines. Thus, there is an interest in discovering the full range of arsenic's potential as a chemotherapeutic and several clinical trials have been initiated to test the efficacy of arsenic in treating solid tumors (Murgo, 2001).

Arsenite is a mitotic disruptor causing mitotic arrest and subsequent apoptosis in SV40-transformed human fibroblast (States *et al.*, 2002), TR9-7 cells (Taylor *et al.*, 2006), HeLa, KB (Huang and Lee, 1998), CGL-2 (Yih *et al.*, 2005), and U937 (McCabe, Jr. *et al.*, 2000;McCollum *et al.*, 2005) cells. The mechanism through which arsenite causes mitotic arrest is highly disputed. Most explanations focus on tubulin as the direct target of arsenite, however much conflict exists in the literature debating whether the mechanism involves tubulin stabilization (Huang and Lee, 1998;Ling *et al.*, 2002), inhibition of tubulin polymerization (Ramirez *et al.*, 1997;Li and Broome, 1999;Carre *et al.*, 2002;Kligerman *et al.*, 2005), or even if there is any effect on tubulin polymerization/organization at all (Li and Chou, 1992;Halicka *et al.*, 2002). Thus, the mechanism for arsenite-induced mitotic arrest is still unresolved.

In this study we directly compared arsenite treatment to a known inhibitor of tubulin polymerization, nocodazole, and a known enhancer of tubulin polymerization, paclitaxel. Most previous studies attempting to elucidate the mechanism of arsenite-induced mitotic arrest have used only one cell line per study. Different cell lines may undergo arsenite-induced mitotic arrest associated apoptosis in distinct sub-phases of mitosis suggested by different apparent morphologies when analyzing tubulin architecture. This variability may partially explain the contrasting results in the current literature. We have used multiple cell lines with differing p53 functionality, a key tumor suppressor gene involved in cell cycle checkpoints and potential escape from mitotic arrest, in order to find factors common among the cell lines tested contributing to arsenite-induced mitotic arrest and cell death. We used two cancer cell lines known to undergo arsenite-induced mitotic arrest and subsequent apoptosis one having functional p53 (melanoma, A375) and and the other phenotypically null p53 (cervical cancer, HeLa) as well as an arsenite-sensitive fibroblast cell line with a tet-off regulated p53 construct (TR9-7). P53 expression has previously been shown to affect the ability of cells to escape from mitotic arrest (Taylor *et al.*, 2006;McNeely *et al.*, 2006). Mitotic structure and protein expression were analyzed in order to identify an alternative mechanism(s) or target(s) unique to arsenite-induced mitotic arrest. Tubulin organization and the mitotic spindle apparatus were examined in all cell lines. Centrosome location and quantity as well as proteins involved in centrosome regulation and organization were examined in order to further examine the mitotic spindle architecture and its organization. We determined that cell morphology and mitotic spindle morphology differ between cells treated with arsenite and the microtubule specific drugs, paclitaxel and nocodazole, and appear to be independent of effects on microtubule polymerization. In addition, we show that only arsenite induced a hyperthermia-like stress response, and inhibition of a key modulator of this response results in an increase in arsenite-induced mitotic arrest, abnormal spindle morphology and cell death.

Materials and Methods

Cell Culture and Specialty Chemicals

All cell cultures were maintained at 37° C at 5% CO_2 and 95% humidity. TR9-7 cells were the kind gift of Dr. Michael A. Tainsky (Wayne State University). Cells were cultured and p53 expression was modulated by direct addition of tetracycline (Sigma Chemical Co., St. Louis, MO) as described previously (Taylor *et al.*, 2006). HeLa CCL-2 cells were a gift from Dr. W. Glenn McGregor (University of Louisville, Louisville, KY) and were cultured in Dulbecco's modified Eagle's medium (Mediatech Inc., Herndon, VA) supplemented with 10% FBS (Hyclone, Logan, UT) and 100 U/ml penicillin with 0.1 mg/ml streptomycin (Cambrex

Bioscience, East Rutherford, NJ). A375 cells were obtained from Dr. Donald L. Miller (University of Louisville, Louisville, KY) and cultured in : Dulbecco's modified Eagle's medium supplemented with 10% FBS and 100 U/ml penicillin with 0.1 mg/ml streptomycin. Working aqueous solutions of $NaAsO_2$ (Sigma) were prepared freshly on the day of treatment and filter sterilized prior to use. TRISENOX® (Arsenic trioxide, ATO) consists of 1.0 mg/mL arsenic trioxide (5 μM ATO), 1.2 mg/ml (30 μM) sodium hydroxide to allow solubility and hydrochloric acid to adjust pH. Every mole of ATO in solution is equivalent to 2 moles of sodium arsenite. The most stable structure of trivalent arsenic oxides existing in solution at neutral pH is $As(OH)_3$ (Ramirez-Solis *et al.*, 2004). Therefore we used sodium arsenite in all experiments for its convenience, ease of use, and identical structure of ATO and sodium arsenite in solution. Stock and working solutions of nocodazole (EMD Biosciences, San Diego, CA) and paclitaxel (Sigma) were prepared in dimethyl sulfoxide (Fisher Scientific, Pittsburgh, PA) and stored in desiccators at -20° C until usage. Stock and working solutions of 17-(Dimethylaminoethylamino)-17-demethoxygeldanamycin (17-DMAG, NSC 707545) (InvivoGen, San Diego, California) were prepared in sterile distilled deionized H_2O and stored protected from light at -20° C until usage.

Immunofluorescence

Adherent cells were grown on poly-D-lysine slides (BD Biosciences, San Jose, CA) prior to fixation and staining. Mitotic and floating cell fractions were harvested via mitotic shake prior to subsequent adherence to poly-D-lysine slides. Shaken cells were added to fresh poly-D-lysine slides and centrifuged at 100 x g for 2 min to aid in cell adherence. Cells attached to slides were washed twice with phosphate buffered saline (PBS) for 5 min before fixation in 4% paraformaldehyde (Sigma) in PBS at 4° C for 15 min. Cells were washed twice with PBS for 5 min followed by 100% methanol (Fisher Scientific) for 10 min at -20 °C. Cells were permeabilized with two washes of PBS containing 0.2% Triton X-100 (Fisher Scientific) for 5 min and blocked with 10% normal goat serum (Sigma) in PBS for 1 hour. Antibodies were preconjugated with either 5 μl AlexaFluor 594 or 488 Zenon reagent (Molecular Probes, Invitrogen, Eugene, Oregon) (Fab fragment) per μg antibody for 5 min before remaining unbound Fab fragments were conjugated to excess non-specific antibody for 5 min. Cells were stained with conjugated antibody for 1 hour in a humidified room temperature chamber. Cells were washed twice with PBS for 5 min before a secondary fixation in 4% formaldehyde (Fisher Scientific) in PBS for 10 min. Cells were again washed twice with PBS and mounted on glass slides with SlowFade® Gold antifade reagent containing DAPI (Molecular Probes, Invitrogen). Slides were stored in the dark at 4 °C until fluorescence microscopy examination. Antibodies used to identify cellular proteins were mouse monoclonal antibodies for histone H3 phosphorylated on serine 10 (Histone H3-S10-P) (Cell Signaling Technology, Inc., Beverly, MA), α-tubulin (Upstate Cell Signaling Solutions, Chicago, IL), and γ-tubulin (Abcam Inc., Cambridge, MA). Pictures were taken using an Olympus IX50 inverted fluorescence microscope (Olympus America Inc., Center Valley, PA) with QImaging Retiga EXi Fast 1394 12-bit cooled monochromatic camera (QImaging Corp., Burnaby, BC, Canada) and examined via Northern Eclipse Image Analysis Software (Empix Imagine, North Tonawanda, NY). Representative examples of three independent experiments were analyzed.

Nuclear Morphology Index Determination

Cells were harvested for mitotic index as previously described (Taylor *et al.*, 2006). Slides were examined under a microscope and at least 900 cells were counted on each slide for determination of mitotic index (MI), mitotic catastrophe index (MCI), and nuclear fragmentation index (NFI). Only cells with distinct interphase nuclei, metaphase spreads, fragmented nuclei or mitotic catastrophe appearance were counted. Three independent experiments were analyzed. DAPI stain in mounting media (Molecular Probes) added directly

to slides was used to verify DNA in interphase nuclei, mitotic spreads, fragmented nuclei and mitotic catastrophe by fluorescence microscopy.

Viability Assays

AlamarBlue measurement of cell viability was performed as described (Nociari *et al.*, 1998). Drug concentration-response data are reported as percent fluorescence of the untreated control versus concentration of drug. Three independent experiments were analyzed and results are shown as average ± standard deviation.

Heat Shock Treatment

To induce heat shock, cells plated in T-25 cell culture flasks were incubated in a 39° C incubator at 5% CO_2 and 95% humidity for 1 h and allowed to recover in a 37° C incubator at 5% CO_2 and 95% humidity for the appropriate times before harvesting.

Western Blot Analysis

Adherent cells, cells floating in media, and washes were collected and washed with PBS. Total cellular lysates were prepared by directly lysing the cells with 200 μL lysis buffer [10 mM Tris-HCl, pH 7.4, 1 mM disodium ethylenediamine tetraacetic acid, 0.1% SDS, 180 μg/mL phenylmethylsulphonyl fluoride per 10 cm dish. Protein concentration was determined by Bradford assay (BioRad, Hercules, CA). Proteins were resolved by sodium dodecylsulfate - polyacrylamide gel electrophoresis (SDS-PAGE) in 12% polyacrylamide gels and transferred to supported nitrocellulose membranes by electroblotting. All western blot analyses contained 10-20 μg protein/lane depending on the cell line used. Proteins were visualized by probing membranes with mouse monoclonal antibodies for α-tubulin (Upstate Cell Signaling Solutions), survivin (Novus Biologicals Inc., Littleton, CO), caspase 2, HSP90 (F-8, Santa Cruz Biotechnology, Santa Cruz, CA), HSP70i (Hsp72, SPA-810, Stressgen Bioreagents, Ann Arbor, MI) and β-actin (Sigma), or rabbit polyclonal antibodies for Histone H2A.X-S139-P, cleaved caspase 3, PARP, Bcl-2, Bcl-2-S70-P, HSP70, (Cell Signaling Technology, Inc.), caspase 8 (H-134, Santa Cruz Biotechnology), and HSP60 (Chemicon International, Millipore, Temecula, CA). Binding of secondary HRP rabbit anti-mouse antibody and goat anti-rabbit antibody (Zymed, San Francisco, CA) was detected by enhanced chemiluminescence (Amersham Biosciences, Piscataway, NJ). β-actin was used as a loading control. Western blots shown are representative of three independent experiments. Blot images were quantified using ImageQuant software and normalized to β-actin. Statistical analysis was performed using two tailed student's t-test with SlideWrite software. All blots were stained with Ponceau S (Acros Organics USA) prior to antibody probing. Ponceau S staining was used to check for equal loading, quality of transfer, and potential normalization for quantification.

Statistical Analysis

Comparison of mitotic indices, centrosome number per mitotic cell quantification, western blot densitometric quantification and IC50 calculations were performed by two tailed student t-test using SlideWrite software.

Results

Morphological analysis of non-mitotic cells treated with arsenite, nocodazole and paclitaxel

TR9-7 and HeLa were used for analyzing non-mitotic adherent cell morphology due to the presence of large cell body extensions (both) and large cell size (TR9-7), allowing for easy visualization of changes in cell shape and tubulin architecture. A375 are not shown due to their small size and round shape with minimal cell body extensions, however results were consistent with HeLa and TR9-7 cells for all of the following studies (not shown). Cells were treated with

arsenite (1-100 μM), nocodazole (1-100 ng/ml), and paclitaxel (1-100 nM) and examined via phase contrast microscopy at 0, 1 and 6 h. Nocodazole and paclitaxel changed adherent cell morphology as early as 1 h after treatment at concentrations as low as 30 ng/ml and 7 nM, respectively (Supplementary Data). The change in morphology can be described as loss of cell body extensions and a switch from a long and slender cell shape to short and round. Arsenite treatment did not change morphology of adherent cells at any concentration after one hour (Supplementary Data). Arsenite (≥ 2.5 μM), nocodazole (≥10 ng/ml) and paclitaxel (≥3 nM) treatments all began to induce a large number of floating cells from 12-24 h due to mitotic arrest and subsequent apoptosis. The change in morphology in nocodazole- and paclitaxel-treated cells was likely due to disruption of tubulin which influences cell architecture. Arsenite did not change adherent cell morphology even at supra-therapeutic concentrations at any time tested in either cell line. Immunofluorescence analysis of α-tubulin after 1 hour treatment in both TR9-7 and HeLa cells show that paclitaxel induced bright staining of hyperpolymerized microtubule bundles while nocodazole induced diffuse staining and cells lacked microtubule fibers (Figure 1 A and B). However, arsenite did not inhibit or induce tubulin polymerization and microtubule fibers appeared unchanged as compared to untreated cells (Figure 1 A and B). It could be argued that unlike nocodazole and paclitaxel, arsenite is not entering or accumulating in the cells at such early time points to affect tubulin polymerization. However, studies have shown that arsenic in the form of arsenic trihydroxide ($As(OH)_3$), the water soluble form of arsenite, enters cells rapidly through human aquaglyceroporins (hAQP9 and hAQP7) (Liu *et al.*, 2004). In addition, non-ionic arsenite transport appears to be involved in the cellular uptake process while ionic transport does not (Ramirez-Solis *et al.*, 2004). We have shown that arsenite accumulates in A375 and SK-Mel-28 cells and that inhibition of arsenite detoxification and metabolism increases arsenic accumulation (McNeely *et al.*, 2008). It is clear that arsenite induces HSP70i as early as 1 hour (Figure 1C). It is possible that this induction is the result of arsenite stimulation of an extracellular signaling process. We have shown that induction of heme oxygenase mRNA (a prototypical component of the stress response) occurs in TR9-7 cells within 3 h of arsenite exposure (McNeely *et al.*, 2006). Thus, arsenite induction of HSP70i is more likely to be an intracellular rather than extracellular signaling process. Neither, nocodazole nor paclitaxel induce HSP70i expression even after 24 h treatment (Figure 4).

Spindle morphology is distinctly different after each drug treatment

In order to observe effects of the three drugs on mitotic tubulin organization, TR9-7, HeLa, and A375 cells were treated with arsenite, nocodazole or paclitaxel for 15 h before mitotic cells were shaken loose, collected and adhered to poly-D-lysine slides. Cells were stained for α-tubulin and histone H3-S10-P mitotic marker and observed via immunofluorescence. Results from HeLa cells are shown in Figure 2. Untreated cells demonstrated clear bipolar spindles in mitosis (Figure 2, row 1). Nocodazole treatment caused mitotic arrest at prophase or prometaphase where mitotic cells lacked a mitotic spindle due to inhibition of tubulin polymerization (Figure 2, row 2). Very short microtubule strands were sometimes assembled at the kinetochores and centrosomes of pro-metaphase mitotic cells giving the tubulin stain a speckled appearance in the nuclei of HeLa (Figure 2), TR9-7, and A375 cells (supplementary data). These data are consistent with reports that nocodazole induces mitotic arrest at prophase and early prometaphase (Rieder and Cole, 2000;Tirnauer *et al.*, 2002), while short microtubules are observed at the kinetochores and centrosomes (De Brabander *et al.*, 1981). Paclitaxel treatment at a chemotherapeutic concentration of 100 nM caused a rigid arrest at metaphase with brightly staining mitotic spindles usually radiating from a central focus appearing as a mono-polar spindle (Figure 2, row 3). Arsenite did not inhibit tubulin polymerization and spindle formation in any cell line but caused the appearance of multi-polar spindles in the majority of mitotic cells in all three cell lines (Figure 2, row 4 and figure 3A, row 4).

Cells were then stained for γ-tubulin and mitotic marker under the same conditions. HeLa cells stained clearly and intensely for γ-tubulin, while A375 cells stained clearly but less intensely. TR9-7 cells have inconsistent staining due to either poor centrosome staining combined with either nonspecific staining or highly fragmented centrosomes even in untreated mitotic TR9-7 cells. Only HeLa cells are shown in Figure 3A, but quantitative data for both HeLa and A375 cells are shown in Figure 3B. Immunofluorescence analysis of mitotic A375 cell γ-tubulin morphology supports data from HeLa cells (Supplemental Data). Untreated cells had two centrosomes in mitotic cells and one or two centrosomes in interphase cells depending on whether cells were in G1 or G2 cell cycle stages, respectively (Figure 3A, row 1 and Figure 3B). Nocodazole-treated mitotic cells also contained two centrosomes (Figure 3A, row 2 and Figure 3B). Without a mitotic spindle providing structure for centrosomal location, the centrosomes were randomly distributed throughout the mitotic cells lacking a spindle.

Paclitaxel (100 nM) produced mitotic cells containing 2 centrosomes (Figure 3A, row 3 and Figure 3B). Mitotic cells either had two centrosomes, one on each side of a metaphase plate, or as a central doublet resulting in a mono-polar spindle with the DNA distributed in a circle around the perimeter of the cell (Figure 3A, row 3). Arsenite, on the other hand, caused centrosome amplification in the majority of mitotic HeLa cells and in almost half of mitotic A375 cells (Figure 3A, row 4, and Figure 3B).

Arsenite treated cells had a wider variety of mitotic morphologies. Unlike nocodazole and paclitaxel treatment, the mitotic stages observed after arsenite treatment ranged from prophase and metaphase to attempted anaphase with lagging DNA between the poles as well as mitotic cells with multiple centrosomes (Supplementary data). All arsenite-treated interphase cells contained either one (G1) or two (G2) centrosomes (not shown). Thus, centrosome amplification occurred after entry into mitosis and appears to occur as cells attempt anaphase. These experiments were repeated using DAPI stain combined with both α- and γ-tubulin together to verify that γ-tubulin was indeed localized at the spindle poles (supplemental data) as previously indicated.

Protein markers of mitotic arrest and apoptosis

TR9-7 cells expressing or not expressing p53, HeLa, and A375 cells were treated for 24 h with 5 μM $NaAsO_2$, 90 ng/ml nocodazole, 7 nM or 100 nM paclitaxel. Lysates were collected after 24 h continuous exposure and analyzed by western blot for protein markers of apoptosis, cell stress and cell cycle regulation (Figure 4). Probing for p53 revealed p53 expression in A375 and in $p53^{(+)}$ TR9-7 cells, but not in HeLa or $p53^{(-)}$ TR9-7 cells (not shown). When analyzing protein markers of apoptosis, cleaved caspase 3 was present in all treated samples in all cell lines. In TR9-7 cells, p53 expression was associated with less caspase 3 cleavage as previously published (Taylor *et al.*, 2006). In all cell lines except HeLa, 7 nM paclitaxel resulted in less caspase 3 cleavage than all other treatments. Presence of PARP cleavage correlated with presence of caspase 3 cleavage. No caspase 8 cleavage was observed under any condition, consistent with the intrinsic pathway of apoptosis initiation (not shown). Caspase 2 cleavage, associated with genotoxic-stress associated cell death, was seen only in A375 cells in each treatment condition, but the most intense cleavage occurred during arsenite treatment (not shown). Bcl-2, an anti-apoptotic protein, remained constant in both A375 and HeLa cells. HeLa cells robustly expressed Bcl-2, possibly explaining minimal caspase 3 cleavage. Bcl-2 in TR9-7 cells decreased in conditions resulting in caspase 3 cleavage. Bcl-2 phosphorylated on serine 70 (Bcl-2-S70-P) appeared during conditions resulting in caspase cleavage, despite decreased overall Bcl-2 levels. Bcl-2 phosphorylation specifically on serine 70 has been associated with positive regulation of Bcl-2 and anti-apoptotic functions (Ito *et al.*, 1997). However, Bcl-2 phosphorylation hinders survival function in paclitaxel-induced apoptosis associated with mitotic arrest (Yamamoto *et al.*, 1999). Histone H2A.X phosphorylation is associated with

DNA double strand breaks. Histone H2A.X phosphorylated on serine 139 (H2A.X-S139-P) was induced by all treatment conditions and induction correlated with caspase 3 and PARP cleavage suggesting that Histone H2A.X was phosphorylated during apoptosis as DNA is cleaved and degraded. Survivin, normally an anti-apoptotic protein, plays an important role in mitosis and mitotic catastrophe (Castedo *et al.*, 2004) and also was induced with treatments resulting in caspase 3 and PARP cleavage.

HSP60, a mitochondrial protein associated with protection from apoptotic cell death, was decreased in TR9-7 cells treated with arsenite and nocodazole. HSP60 remained unchanged in other cell lines and treatments (not shown). HSP70 induction is a typical stress response and is involved in prevention of apoptosis from heat shock insult. The HSP70 antibody detects both constitutive 73 kDa and inducible 72 kDa heat shock proteins. Arsenite, but not nocodazole or paclitaxel treatment, induced a 72 kDa HSP70 protein consistently in all cell lines. HeLa cells had a higher baseline expression of the lower 72 kDa HSP70 protein making it difficult to distinguish between the 73 and 72 kDa proteins. Arsenite induction of inducible HSP70i was confirmed by probing with an HSP70i (72 kDa) specific antibody. HSP70i induction by arsenite was significantly induced above untreated control levels as well as all other treatment conditions in all cell lines tested (quantitiation of western blots is presented in supplemental data). Any HSP70i induction by other treatments was inconsistent (supplemental data). HSP90 was expressed in all cell lines and changes in expression with treatment were not statistically significant (supplemental data). α-tubulin levels also were not affected by any treatment condition. β-actin was used as a loading control and was unaffected by all treatment conditions as well.

Heat shock induces centrosome amplification

HeLa cells were subjected to heat shock for 1 h at 39 °C. Mitotic cells were harvested at 0, 1, 3 and 6 h post-heat shock and analyzed via immunofluorescence for centrosome quantitation. Heat shock induced mild abnormal centrosome amplification in mitotic cells which appeared similar in morphology to arsenite-treated mitotic cells (Figure 5A.). Abnormal centrosome number peaked at 1 h post-heat shock and decreased over time (Figure 5B). Abnormal centrosome number at 1 h post heat shock was significantly higher than in untreated (pre-heat shock) cells and 6 h post heat shock treated cells ($p < 0.01$). Induction of HSP70i peaks at 3 h post recovery and correlates with recovery of abnormal centrosome number from 3 to 6 h (Figure 5C).

Disruption of HSP70/HSP90 activity enhances effectiveness of arsenite

HSP70i knockdown using siRNA sensitized HeLa cells to arsenite treatment and increased arsenite-induced abnormal centrosome amplification. However, the changes, despite being consistent between study methods, were not statistically significant (supplementary data). Lack of statistical significance could be due to the presence of constitutive HSP70, HSP90, and other constitutive or inducible HSP and HSP-like proteins capable of protecting the cell from arsenite treatment. Both HSP90 and HSP70 are located at and help regulate the centrosome during mitosis (Rattner, 1991;de Carcer *et al.*, 2001). HSP70 and HSP90 work cooperatively in a complex (Schumacher *et al.*, 1996;Hernandez *et al.*, 2002). Thus, direct inhibition of HSP90 may have a much more profound effect on arsenite sensitivity and centrosome regulation than preventing induction of HSP70i. A375, HeLa and TR9-7 ($p53^{(-)}$) cells were plated in 96 well dishes and treated for up to 3 days with 0-300 nM 17-DMAG (a potent inhibitor of HSP90 ATPase activity, (Eiseman *et al.*, 2005)) combined with either 0, 0.5, 1, 2.5 or 5 μM arsenite. Viability was measured using AlamarBlue after 48 h of treatment (Figure 6). Top graphs represent 17-DMAG dose response while bottom graphs show arsenite dose response. In HeLa cells, addition of low level arsenite concentrations (1, 2.5 and 5 μM) enhanced cytotoxicity of 17-DMAG specifically at 10 nM 17-DMAG (Figure 6, top graphs). Addition of 1 and 2.5 μM

arsenite alone results in 6.4 and 21.4% decreases in cell viability respectively, while 10 nM 17-DMAG alone resulted in a 12.6% decrease in viability. Combining 10 nM 17-DMAG with 1 and 2.5 μM arsenite resulted in 38.1 and 67.4% decreases in viability, respectively, indicating supra-additive inhibition. In A375 and TR9-7 cells, addition of low level arsenite (0.5, 1 and 2.5 μM) increases cytotoxicity of 17-DMAG specifically at 10 nM 17-DMAG and 10-30 nM DMAG respectively (Figure 6, top graphs). In A375 cells, addition of 1 μM arsenite alone results in a 19.7% decrease in viability while 10 nM 17-DMAG alone resulted in a 29.3% decrease in viability. Combining 10 nM 17-DMAG with 1 μM arsenite resulted in 62.3% decrease in viability, indicating a supra-additive effect. Finally, in TR9-7 cells, addition of 1 and 2.5 μM arsenite alone results in a 15.1 and 45.2% decrease in viability, respectively, while 10 nM 17-DMAG alone resulted in a 5.9% decrease in viability. Combining 10 nM 17-DMAG with 1 and 2.5 μM arsenite resulted in a 32.8 and 58.6% decrease in viability, respectively, also indicating a supra-additive effect. This effect is more apparent when arsenite dose response is shown (Figure 6, bottom graphs). Ten nM 17-DMAG enhances the response of A375 to arsenite treatments, while 3 and 10 nM 17-DMAG enhances the response of HeLa cells to arsenite treatments. The response to arsenite treatments in TR9-7 cells are enhanced by 10-30 nM DMAG. The supra-additive effect shown at low levels of arsenite combined with 17-DMAG is corroborated by IC50 calculations. Arsenite-induced changes in 17-DMAG IC50 (Table 1, top row) as well as 17-DMAG-induced changes in arsenite IC50 (Table 1, bottom row) were shown to be statistically significant in each cell line as labeled.

Mitotic index analysis revealed a 17-DMAG dose response where 10 nM alone causes modest increase in mitotic cells in both A375 and HeLa cells (5.1 and 6.5%, respectively) and 30 nM 17-DMAG causes more robust mitotic arrest (18.0 and 15.0%, respectively) (Figure 7A). Three μM arsenite treatment in A375 cells and 5 μM arsenite treatment in HeLa cells induced mitotic indices of 11.3 and 11.1%, respectively (Figure 7A). Combined treatment of 10 nM 17-DMAG with 3 μM arsenite treatment in A375 cells or 5 μM arsenite treatment in HeLa cells induced a mitotic indices greater than either treatment alone (18.5 and 20.7%, respectively), resulting in a supra-additive effect (Figure 7A). Combined treatment also induced a mitotic arrest accumulation greater than increasing 17-DMAG alone to 30 nM. Incidence of mitotic catastrophe also increased slightly in the combined treatment relative to either treatment alone in both cell lines. Ten and 30 nM 17-DMAG induced mitotic centrosome abnormalities in A375 (14.3 and 22.8% respectively) and HeLa cells (14.6 and 28.3%, respectively) (Figure 7B). Centrosome abnormalities induced by 17-DMAG alone were small relative to arsenite alone and arsenite in combination with 10 nM 17-DMAG. Furthermore, combining 10 nM 17-DMAG with arsenite enhanced induction of arsenite-induced centrosome abnormalities (Figure 7B). Combined treatment of arsenite and 10 nM 17-DMAG resulted in more centrosome abnormalities than arsenite treatment alone in both A375 (59.3 vs. 37.0%) and HeLa (67.4 vs. 47.1%), indicating a supra-additive effect on centrosome abnormalities as well. Western blot analyses (Figure 8C) revealed that, as in Figure 4, arsenite alone induced very robust PARP and caspase cleavage, indicative of apoptosis. Neither concentration of 17-DMAG given alone induced significant PARP or caspase 3 cleavage. Combined arsenite and 10 nM 17-DMAG increased the levels of PARP and caspase cleavage relative to arsenite treatment alone. No consistent changes were seen in total HSP90 levels with arsenite or 17-DMAG treatment alone or in combination.

Discussion

Arsenite (administered as Trisenox®) is a useful chemotherapeutic, approved for ATRA refractory APL, that could replace or be used in combination with other drugs as first-line treatment for APL (Raffoux *et al.*, 2003;Shen *et al.*, 2004;Hede, 2007) and potentially in the treatment of other malignancies. The mechanism of arsenite-induced mitotic arrest and subsequent apoptosis is controversial. Arsenite has been reported to inhibit, to promnote and

to have no effect on tubulin polymerization. Understanding the mechanism of arsenite-induced mitotic arrest is an important step guiding new drug design as well as design of treatments combining arsenic with other drugs. Our results support the hypothesis that arsenite-induced mitotic arrest involves a novel mechanism. Identifying the target(s) of arsenite will provide new and more selective targets for drug design and development. In this article, we address this issue by directly comparing arsenite induced-mitotic arrest with well-characterized spindle poisons that both stabilize (paclitaxel) and destabilize (nocodazole) microtubules.

Our first indication that arsenite was working through a unique mechanism compared to tubulin disrupting drugs, was from observation of cell morphology with light microscopy (Supplementary Data). Nocodazole and paclitaxel induced rapid changes in cell morphology in both cell lines tested (Figure 1 A and B). These drugs caused a loss of cellular extensions and rounded cell shape. Arsenite had no effect on adherent cell morphology at any time point up to 24 h at chemotherapeutic concentrations (2-5 μM) or even at supra-therapeutic concentrations of 30 – 100 μM up to 6 h. Arsenite has been reported to disrupt both actin and tubulin at concentrations above 20 μM in more extended exposures (Li and Chou, 1992). Using immunofluorescence staining of α-tubulin we were able to determine that arsenite, sufficient to induce mitotic arrest, does not affect tubulin architecture whereas nocodazole and paclitaxel clearly disrupt and hyper-stabilize tubulin, respectively.

When analyzing the mitotic spindle we used concentrations of arsenite (5 μM), nocodazole (90 ng/ml) and paclitaxel (100 nM) previously determined to induce a high percentage of mitotically arrested cells. Through immunofluorescence analysis, it was clear in all cell lines that nocodazole induced a mitotic arrest with the absence of spindle formation (Figure 2). Paclitaxel at both low and high concentrations allowed formation of spindles staining brightly for α-tubulin. High concentration paclitaxel resulted in many apparently mono-polar spindles (Figure 2). A commonly suggested mechanism of arsenite-induced mitotic arrest is based on arsenite inhibiting tubulin polymerization through sulfhydryl binding in the GTP binding site of β-tubulin (Ramirez *et al.*, 1997;Li and Broome, 1999;Carre *et al.*, 2002;Kligerman *et al.*, 2005). On the contrary, we observed clear formation of a mitotic spindle apparatus in all arsenite-treated mitotic cells, in contrast to nocodazole-treated cells (Figure 2). In our experiments anaphase arrest was observed in cells treated with arsenite but not nocodazole or paclitaxel (Supplementary data). Arsenite produced a large fraction of cells with abnormal and multi-polar spindles as well as cells attempting anaphase with unsuccessful separation of chromatids. This observation prompted us to pursue the centrosome and proteins involved in centrosomal regulation as targets for arsenite induced mitotic arrest. Immunofluorescence analysis of γ-tubulin demonstrated that of the 3 drugs tested, only arsenite produced abnormal centrosome number (>2) in the majority of mitotic cells in both HeLa and A375 cells (Figure 3A and C). Abnormal centrosome number was also observed in arsenite-treated CGL-2 cells and was dependent on the spindle assembly checkpoint (SAC) and increased centrosome number correlated with time arrested in mitosis (Yih *et al.*, 2006). All cells used in the curent study had a functional SAC due to the ability of both nocodazole and paclitaxel treatment to induce robust mitotic arrest. Our study confirms and extends this earlier observation, showing the universality of a functional SAC required for mitotic arrest.

The minimally effective plasma paclitaxel concentration in patients is reported to be 100 nM (Sekine *et al.*, 1996;Malingre *et al.*, 2001;Mross *et al.*, 2006;Kobayashi *et al.*, 2006). Both 100 and 7 nM paclitaxel concentrations were analyzed but only immunofluorescence data from cells treated with 100 nM paclitaxel were shown. Surprisingly, low paclitaxel concentrations caused a significant increase in centrosome number in HeLa but not A375 cells in our experiments. Low paclitaxel was the only other treatment in our studies capable of inducing abnormal centrosome amplification, although significantly less than the amount caused by arsenite treatment. Cell death at concentrations less than 9 nM paclitaxel occurred through a

different mechanism (aberrant mitosis) than the mechanism postulated to occur at concentrations above 9 nM (terminal mitotic arrest, Raf-1-dependent) (Torres and Horwitz, 1998). It may be that low paclitaxel more specifically affects spindle pole formation, while higher paclitaxel concentrations result in a more rigid mitotic arrest due to severe hyper-polymerization of all tubulin throughout the mitotic spindle. We also observed less evidence of apoptosis in low paclitaxel treatment in our western blot analysis (Figure 4). This decrease in apoptosis may be due to an exit from mitosis without division causing fragmented nuclei (supplementary data) and resulting in G1 arrest and delayed onset of apoptosis. It has been reported that paclitaxel's induction of apoptosis can occur due to aberrant mitosis or to entering a multinucleated G1-like state subsequent to mitotic slippage, depending on cell type and drug schedule (Abal *et al.*, 2003). A recent study reported that high paclitaxel treatment causes well sustained spindle checkpoint activation leading to mitotic block, while low concentrations below 10 nM cause mitotic delay but premature abrogation of the spindle checkpoint leading to aneuploidy (Ikui *et al.*, 2005). We observed a similar phenomenon comparing low and high paclitaxel levels (supplementary data). Thus, despite the observations that the tubulin disrupting drug paclitaxel, can sometimes induce abnormal centrosome amplification in a dose- and cell-dependent manner, arsenite may impair normal centrosome organization directly or through interaction with proteins involved in centrosome organization and function.

A key component of centrosome structure and function is the chaperone heat shock protein HSP70. HSP70 is involved in protein folding and organization of the spindle apparatus (Sconzo *et al.*, 1999;Agueli *et al.*, 2001). There are both constitutive (73 kDa) and inducible (72 kDa) HSP70 isoforms. Induction of HSP70 by arsenite (Liu *et al.*, 2001;Khalil *et al.*, 2006) (Figure 4) is likely a consequence of arsenite's function as a pro-oxidant (Eblin *et al.*, 2006). HSP70 over-expression is reported to protect cells from arsenite induced genotoxicity (Barnes *et al.*, 2002). We (Figure 6) and others (Vidair *et al.*, 1993;Hut *et al.*, 2005) have shown that heat shock (hyperthermia) alone can induce abnormally high centrosome number in mitotic cells. Heat shock delays mitotic progression and HSP70 expression protects against hyperthermia-induced centrosome abnormalities (Vidair *et al.*, 1993;Hut *et al.*, 2005). In our studies, siRNA knockdown experiments investigating the role of HSP70i induction in centrosome amplification were inconclusive (supplemental data). Confounders included the stress of transfection and the constitutive HSP70 which is still present and active which may limit the effects of HSP70i knockdown.

HSP70 activity is dependent on interaction with HSP90. The HSP70/HSP90 complex functions cooperatively with other key proteins in order to organize protein folding and renature damaged proteins (Schumacher *et al.*, 1996;Hernandez *et al.*, 2002). HSP90 and HSP70 are both intimately involved in centrosome regulation and mitotic spindle formation and organization (Liang and MacRae, 1997). We also have shown that HSP70i is localized at the centrosome in mitotic HeLa cells (Supplementary data). HSP90 inhibitors 17-AAG and 17-DMAG are now in clinical trials (Ramanathan *et al.*, 2005;Shadad and Ramanathan, 2006;Nowakowski *et al.*, 2006;Ronnen *et al.*, 2006). A recent study identifies 17-AAG-induced kinetochore defects as a possible mechanism of HSP90 inhibitor-induced mitotic arrest (Niikura *et al.*, 2006). However, HSP90 inhibitors causing disruption or protein defects at the centrosome may be an additional mechanism causing HSP90 inhibitor-induced mitotic arrest and cell death. Similar to arsenite, the HSP90 inhibitor geldanamycin causes cell death through mitotic catastrophe in human glioma cells (Nomura *et al.*, 2004). We also found that the HSP90 inhibitor 17-DMAG produced a mitotic arrest and induction of abnormal centrosome number (Figure 7A and B). More importantly, low concentrations of 17-DMAG (10 nM) enhanced arsenite-induced cytotoxicity, mitotic arrest, and induction of abnormal centrosomes, showing a supra-additive effect between the two drugs (Figures 6 and 7). Thus, HSP90 and HSP70 function at the centrosome to protect cells from arsenite-induced cell death through prevention of centrosome abnormalities and mitotic arrest.

In this article, we have demonstrated that arsenite and microtubule disrupting drugs induce mitotic arrest by different mechanisms. Clear differences between the three drugs suggest that the mechanism of arsenite-induced mitotic arrest and subsequent apoptosis is unlikely to be due to direct effects on microtubule polymerization. The results presented here suggest that the mechanism of arsenite induced mitotic arrest is related to disruption of centrosome function similar to heat shock. Centrosome amplification is a hallmark of cancer cells in culture, thus it may be argued that cancer cells are more susceptible to agents that cause centrosome amplification. However, since HSP90 and both HSP90 and HSP70 are involved in both kinetochore and centrosome organization respectively, disruption of heat shock proteins by arsenite may increase centrosome abnormalities and induce mitotic arrest.

The exact mechanism of arsenite-induced mitotic arrest remains unclear and further investigation into HSP70 induction and its role in arsenite-induced mitotic arrest and centrosome abnormalities is warranted. In addition, further investigation into the effects of inhibition of HSP90 on arsenite treatment is also warranted, due to HSP90's association with HSP70 and the centrosome.

Supplementary Material

Refer to Web version on PubMed Central for supplementary material.

Acknowledgements

This work was supported by NIH grants R01 ES011314, T32 ES011564, F30 ES013372 and P30 ES014443. Portions of this work constituted partial fulfillment for the Ph.D. in Pharmacology and Toxicology awarded to B. Frazier Taylor from the University of Louisville.

Reference List

Abal M, Andreu JM, Barasoain I. Taxanes: microtubule and centrosome targets, and cell cycle dependent mechanisms of action. Curr Cancer Drug Targets 2003;3:193–203. [PubMed: 12769688]

Agueli C, Geraci F, Giudice G, Chimenti L, Cascino D, Sconzo G. A constitutive 70 kDa heat-shock protein is localized on the fibres of spindles and asters at metaphase in an ATP-dependent manner: a new chaperone role is proposed. Biochem J 2001;360:413–419. [PubMed: 11716770]

Amadori S, Fenaux P, Ludwig H, O'dwyer M, Sanz M. Use of arsenic trioxide in haematological malignancies: insight into the clinical development of a novel agent. Curr Med Res Opin 2005;21:403–411. [PubMed: 15811209]

Antman KH. Introduction: the history of arsenic trioxide in cancer therapy. Oncologist 2001;6:1–2. [PubMed: 11331433]

Barnes JA, Collins BW, Dix DJ, Allen JW. Effects of heat shock protein 70 (Hsp70) on arsenite-induced genotoxicity. Environ Mol Mutagen 2002;40:236–242. [PubMed: 12489113]

Carre M, Carles G, Andre N, Douillard S, Ciccolini J, Briand C, Braguer D. Involvement of microtubules and mitochondria in the antagonism of arsenic trioxide on paclitaxel-induced apoptosis. Biochem Pharmacol 2002;63:1831–1842. [PubMed: 12034367]

Castedo M, et al. Mitotic catastrophe constitutes a special case of apoptosis whose suppression entails aneuploidy. Oncogene 2004;23:4362–4370. [PubMed: 15048075]

Cohen MH, Hirschfeld S, Flamm HS, Ibrahim A, Johnson JR, O'Leary JJ, White RM, Williams GA, Pazdur R. Drug approval summaries: arsenic trioxide, tamoxifen citrate, anastrazole, paclitaxel, bexarotene. Oncologist 2001;6:4–11. [PubMed: 11161223]

De Brabander M, Geuens G, De Mey J, Joniau M. Nucleated assembly of mitotic microtubules in living PTK2 cells after release from nocodazole treatment. Cell Motil 1981;1:469–483.

de Carcer G, do Carmo AM, Lallena MJ, Glover DM, Gonzalez C. Requirement of Hsp90 for centrosomal function reflects its regulation of Polo kinase stability. EMBO J 2001;20:2878–2884. [PubMed: 11387220]

Eblin KE, Bowen ME, Cromey DW, Bredfeldt TG, Mash EA, Lau SS, Gandolfi AJ. Arsenite and monomethylarsonous acid generate oxidative stress response in human bladder cell culture. Toxicol Appl Pharmacol 2006;217:7–14. [PubMed: 16930658]

Eiseman JL, Lan J, Lagattuta TF, Hamburger DR, Joseph E, Covey JM, Egorin MJ. Pharmacokinetics and pharmacodynamics of 17-demethoxy 17-[[(2-dimethylamino)ethyl]amino]geldanamycin (17DMAG, NSC 707545) in C.B-17 SCID mice bearing MDA-MB-231 human breast cancer xenografts. Cancer Chemother Pharmacol 2005;55:21–32. [PubMed: 15338192]

Halicka HD, Smolewski P, Darzynkiewicz Z, Dai W, Traganos F. Arsenic trioxide arrests cells early in mitosis leading to apoptosis. Cell Cycle 2002;1:201–209. [PubMed: 12429934]

Hede K. Chinese folk treatment reveals power of arsenic to treat cancer, new studies under way. J Natl Cancer Inst 2007;99:667–668. [PubMed: 17470732]

Hernandez MP, Sullivan WP, Toft DO. The assembly and intermolecular properties of the hsp70-Hop-hsp90 molecular chaperone complex. J Biol Chem 2002;277:38294–38304. [PubMed: 12161444]

Huang SC, Lee TC. Arsenite inhibits mitotic division and perturbs spindle dynamics in HeLa S3 cells. Carcinogenesis 1998;19:889–896. [PubMed: 9635879]

Hut HM, Kampinga HH, Sibon OC. Hsp70 protects mitotic cells against heat-induced centrosome damage and division abnormalities. Mol Biol Cell 2005;16:3776–3785. [PubMed: 15930131]

Ikui AE, Yang CP, Matsumoto T, Horwitz SB. Low concentrations of taxol cause mitotic delay followed by premature dissociation of p55CDC from Mad2 and BubR1 and abrogation of the spindle checkpoint, leading to aneuploidy. Cell Cycle 2005;4:1385–1388. [PubMed: 16138009]

Ito T, Deng X, Carr B, May WS. Bcl-2 phosphorylation required for anti-apoptosis function. J Biol Chem 1997;272:11671–11673. [PubMed: 9115213]

Khalil S, Luciano J, Chen W, Liu AY. Dynamic regulation and involvement of the heat shock transcriptional response in arsenic carcinogenesis. J Cell Physiol 2006;207:562–569. [PubMed: 16447264]

Kligerman AD, Doerr CL, Tennant AH. Oxidation and methylation status determine the effects of arsenic on the mitotic apparatus. Mol Cell Biochem 2005;279:113–121. [PubMed: 16283520]

Kobayashi M, Sakamoto J, Namikawa T, Okamoto K, Okabayashi T, Ichikawa K, Araki K. Pharmacokinetic study of paclitaxel in malignant ascites from advanced gastric cancer patients. World J Gastroenterol 2006;12:1412–1415. [PubMed: 16552811]

Li W, Chou IN. Effects of sodium arsenite on the cytoskeleton and cellular glutathione levels in cultured cells. Toxicol Appl Pharmacol 1992;114:132–139. [PubMed: 1585365]

Li YM, Broome JD. Arsenic targets tubulins to induce apoptosis in myeloid leukemia cells. Cancer Res 1999;59:776–780. [PubMed: 10029061]

Liang P, MacRae TH. Molecular chaperones and the cytoskeleton. J Cell Sci 1997;110(Pt 13):1431–1440. [PubMed: 9224761]

Ling YH, Jiang JD, Holland JF, Perez-Soler R. Arsenic trioxide produces polymerization of microtubules and mitotic arrest before apoptosis in human tumor cell lines. Mol Pharmacol 2002;62:529–538. [PubMed: 12181429]

Liu J, Kadiiska MB, Liu Y, Lu T, Qu W, Waalkes MP. Stress-related gene expression in mice treated with inorganic arsenicals. Toxicol Sci 2001;61:314–320. [PubMed: 11353140]

Liu Z, Carbrey JM, Agre P, Rosen BP. Arsenic trioxide uptake by human and rat aquaglyceroporins. Biochem Biophys Res Commun 2004;316:1178–1185. [PubMed: 15044109]

Malingre MM, Beijnen JH, Rosing H, Koopman FJ, van Tellingen O, Duchin K, Bokkel Huinink WW, Swart M, Lieverst J, Schellens JH. The effect of different doses of cyclosporin A on the systemic exposure of orally administered paclitaxel. Anticancer Drugs 2001;12:351–358. [PubMed: 11335792]

McCabe MJ Jr, Singh KP, Reddy SA, Chelladurai B, Pounds JG, Reiners JJ Jr, States JC. Sensitivity of myelomonocytic leukemia cells to arsenite-induced cell cycle disruption, apoptosis, and enhanced differentiation is dependent on the inter-relationship between arsenic concentration, duration of treatment, and cell cycle phase. J Pharmacol Exp Ther 2000;295:724–733. [PubMed: 11046111]

McCollum G, Keng PC, States JC, McCabe MJ. Arsenite delays progression through each cell cycle phase and induces apoptosis following G2/M arrest in U937 myeloid leukemia cells. J Pharmacol Exp Ther. 2005

McNeely SC, Belshoff A, Taylor BF, Fan T, McCabe MJ, Pinhas A, States JC. Sensitivity to Sodium Arsenite Depends upon Susceptibility to Arsenite-induced Mitotic Arrest. Toxicol Appl Pharmacol. 2008In Press

McNeely SC, Xu X, Taylor BF, Zacharias W, McCabe MJ Jr, States JC. Exit from arsenite-induced mitotic arrest is p53 dependent. Environ Health Perspect 2006;114:1401–1406. [PubMed: 16966095]

Mross K, Hollander N, Frost A, Unger C, Ziroli V, Massing U. PAC fixed dose: pharmacokinetics of a 1-hour paclitaxel infusion and comparison to BSA-normalized drug dosing. Onkologie 2006;29:444–450. [PubMed: 17028453]

Murgo AJ. Clinical trials of arsenic trioxide in hematologic and solid tumors: overview of the National Cancer Institute Cooperative Research and Development Studies. Oncologist 2001;6:22–28. [PubMed: 11331437]

Niikura Y, Ohta S, Vandenbeldt KJ, Abdulle R, McEwen BF, Kitagawa K. 17-AAG, an Hsp90 inhibitor, causes kinetochore defects: a novel mechanism by which 17-AAG inhibits cell proliferation. Oncogene 2006;25:4133–4146. [PubMed: 16501598]

Nociari MM, Shalev A, Benias P, Russo C. A novel one-step, highly sensitive fluorometric assay to evaluate cell-mediated cytotoxicity. J Immunol Methods 1998;213:157–167. [PubMed: 9692848]

Nomura M, Nomura N, Newcomb EW, Lukyanov Y, Tamasdan C, Zagzag D. Geldanamycin induces mitotic catastrophe and subsequent apoptosis in human glioma cells. J Cell Physiol 2004;201:374–384. [PubMed: 15389545]

Nowakowski GS, McCollum AK, Ames MM, Mandrekar SJ, Reid JM, Adjei AA, Toft DO, Safgren SL, Erlichman C. A phase I trial of twice-weekly 17-allylamino-demethoxy-geldanamycin in patients with advanced cancer. Clin Cancer Res 2006;12:6087–6093. [PubMed: 17062684]

Raffoux E, et al. Combined treatment with arsenic trioxide and all-trans-retinoic acid in patients with relapsed acute promyelocytic leukemia. J Clin Oncol 2003;21:2326–2334. [PubMed: 12805334]

Ramanathan RK, et al. Phase I pharmacokinetic-pharmacodynamic study of 17-(allylamino)-17-demethoxygeldanamycin (17AAG, NSC 330507), a novel inhibitor of heat shock protein 90, in patients with refractory advanced cancers. Clin Cancer Res 2005;11:3385–3391. [PubMed: 15867239]

Ramirez P, Eastmond DA, Laclette JP, Ostrosky-Wegman P. Disruption of microtubule assembly and spindle formation as a mechanism for the induction of aneuploid cells by sodium arsenite and vanadium pentoxide. Mutat Res 1997;386:291–298. [PubMed: 9219566]

Ramirez-Solis A, Mukopadhyay R, Rosen BP, Stemmler TL. Experimental and theoretical characterization of arsenite in water: insights into the coordination environment of As-O. Inorg Chem 2004;43:2954–2959. [PubMed: 15106984]

Rattner JB. hsp70 is localized to the centrosome of dividing HeLa cells. Exp Cell Res 1991;195:110–113. [PubMed: 2055259]

Rieder CL, Cole R. Microtubule disassembly delays the G2-M transition in vertebrates. Curr Biol 2000;10:1067–1070. [PubMed: 10996076]

Ronnen EA, Kondagunta GV, Ishill N, Sweeney SM, Deluca JK, Schwartz L, Bacik J, Motzer RJ. A phase II trial of 17-(Allylamino)-17-demethoxygeldanamycin in patients with papillary and clear cell renal cell carcinoma. Invest New Drugs 2006;24:543–546. [PubMed: 16832603]

Schumacher RJ, Hansen WJ, Freeman BC, Alnemri E, Litwack G, Toft DO. Cooperative action of Hsp70, Hsp90, and DnaJ proteins in protein renaturation. Biochemistry 1996;35:14889–14898. [PubMed: 8942653]

Sconzo G, Palla F, Agueli C, Spinelli G, Giudice G, Cascino D, Geraci F. Constitutive hsp70 is essential to mitosis during early cleavage of Paracentrotus lividus embryos: the blockage of constitutive hsp70 impairs mitosis. Biochem Biophys Res Commun 1999;260:143–149. [PubMed: 10381358]

Sekine I, Nishiwaki Y, Watanabe K, Yoneda S, Saijo N. Phase II study of 3-hour infusion of paclitaxel in previously untreated non-small cell lung cancer. Clin Cancer Res 1996;2:941–945. [PubMed: 9816254]

Shadad FN, Ramanathan RK. 17-dimethylaminoethylamino-17-demethoxygeldanamycin in patients with advanced-stage solid tumors and lymphoma: a phase I study. Clin Lymphoma Myeloma 2006;6:500–501. [PubMed: 16796784]

Shen ZX, et al. All-trans retinoic acid/As2O3 combination yields a high quality remission and survival in newly diagnosed acute promyelocytic leukemia. Proc Natl Acad Sci U S A 2004;101:5328–5335. [PubMed: 15044693]

States JC, Reiners JJ Jr, Pounds JG, Kaplan DJ, Beauerle BD, McNeely SC, Mathieu P, McCabe MJ Jr. Arsenite disrupts mitosis and induces apoptosis in SV40-transformed human skin fibroblasts. Toxicol Appl Pharmacol 2002;180:83–91. [PubMed: 11969375]

Taylor BF, McNeely SC, Miller HL, Lehmann GM, McCabe MJ Jr, States JC. p53 suppression of arsenite-induced mitotic catastrophe is mediated by p21CIP1/WAF1. J Pharmacol Exp Ther 2006;318:142–151. [PubMed: 16614167]

Tirnauer JS, Canman JC, Salmon ED, Mitchison TJ. EB1 targets to kinetochores with attached, polymerizing microtubules. Mol Biol Cell 2002;13:4308–4316. [PubMed: 12475954]

Torres K, Horwitz SB. Mechanisms of Taxol-induced cell death are concentration dependent. Cancer Res 1998;58:3620–3626. [PubMed: 9721870]

Vidair CA, Doxsey SJ, Dewey WC. Heat shock alters centrosome organization leading to mitotic dysfunction and cell death. J Cell Physiol 1993;154:443–455. [PubMed: 8436595]

Waxman S, Anderson KC. History of the development of arsenic derivatives in cancer therapy. Oncologist 2001;6:3–10. [PubMed: 11331434]

Yamamoto K, Ichijo H, Korsmeyer SJ. BCL-2 is phosphorylated and inactivated by an ASK1/Jun N-terminal protein kinase pathway normally activated at G(2)/M. Mol Cell Biol 1999;19:8469–8478. [PubMed: 10567572]

Yih LH, Hsueh SW, Luu WS, Chiu TH, Lee TC. Arsenite induces prominent mitotic arrest via inhibition of G2 checkpoint activation in CGL-2 cells. Carcinogenesis 2005;26:53–63. [PubMed: 15471901]

Yih LH, Tseng YY, Wu YC, Lee TC. Induction of centrosome amplification during arsenite-induced mitotic arrest in CGL-2 cells. Cancer Res 2006;66:2098–2106. [PubMed: 16489010]

Abbreviations

APL
: acute promyelocytic leukemia

ATO
: arsenic trioxide

ATRA
: all-trans retinoic acid

DAPI
: 4′,6-diamidino-2-phenylindole

17-DMAG
: 17-(Dimethylaminoethylamino)-17-demethoxygeldanamycin

FBS
: fetal bovine serum

IC50
: 50% of the maximal inhibitory concentration

MCI
: mitotic catastrophe index

MI
: mitotic index

NFI
: nuclear fragmentation index

NSC
non-specific control

PARP
poly (ADP-ribose) polymerase

PBS
phosphate buffered saline

SD
standard deviation

SDS-PAGE
sodium dodecyl sulfate-polyacrylamide gel electrophoresis

siRNA
small interfering ribonucleic acid

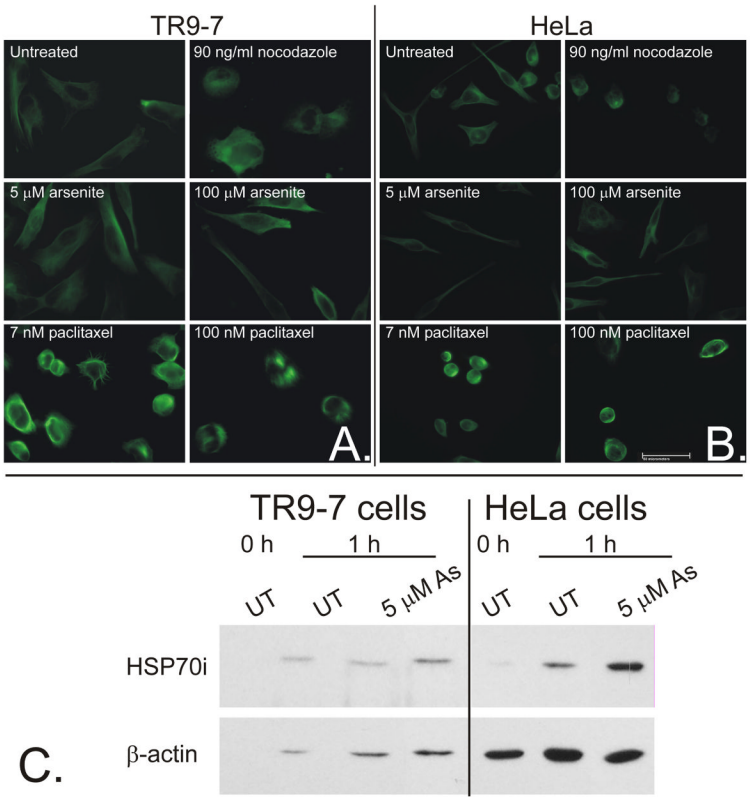

Figure 1. Paclitaxel and nocodazole but not arsenite disrupt adherent cell tubulin architecture after 1 h

A. TR9-7 and **B.** HeLa cells were grown on poly-D-lysine coated coverslips and treated with either nocodazole, paclitaxel or arsenite at the concentrations shown for 1 h before fixation and subsequent staining for cytoskeletal proteins α-tubulin. Cells were analyzed and photographed via fluorescence microscopy. **C.** Both cell lines were treated with 0 or 5 μM arsenite for 1 h and total cellular lysate proteins were resolved by SDS-PAGE, transferred to nitrocellulose membranes, and probed for HSP70i and β-actin.

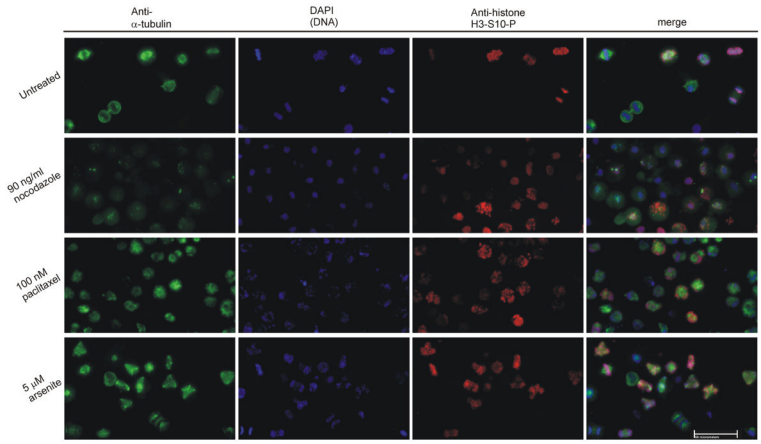

Figure 2. Analysis of spindle in mitotic cells

HeLa cells were grown in drug free media in 15 cm dishes, while cells treated with 90 ng/ml nocodazole, 100 nM paclitaxel, or 5 μM arsenite were grown in 6 cm dishes for 15 h. Detached cells were shaken, pelleted, and adhered to poly-D-lysine slides before fixation and staining with anti-α-tubulin (AlexaFluor 488, green), anti-histone H3-S10-P (a mitotic marker, AlexaFluor 594, red), and DAPI (blue). Cells were analyzed and photographed via fluorescence microscopy. Representative examples of three independent experiments are shown. White bar represents 50 micrometers.

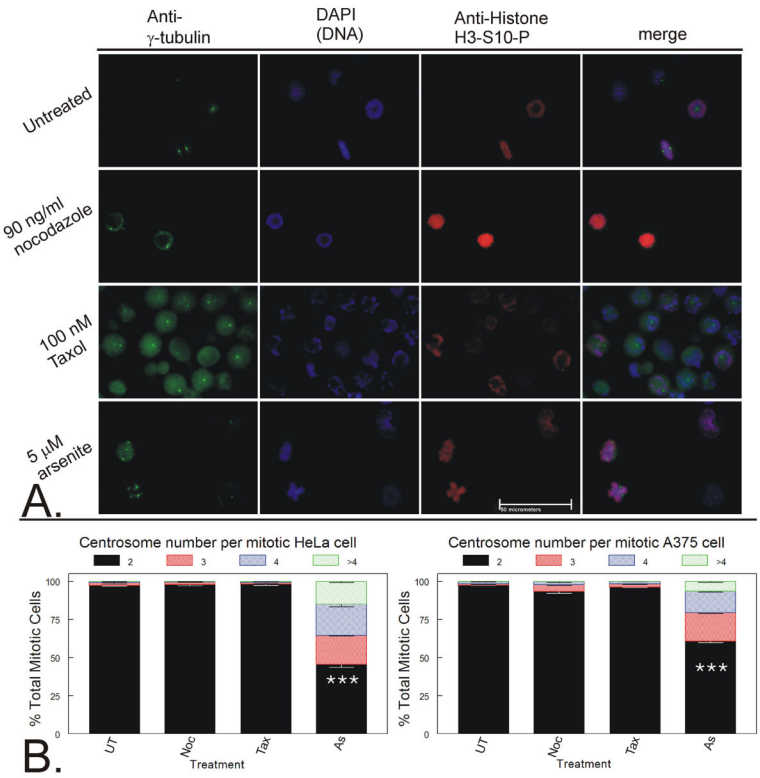

Figure 3. Analysis of centrosome number and location in mitotic cells

A. HeLa cells were grown in drug free media in 15 cm dishes, while cells treated with 90 ng/ml nocodazole (Noc 100 nM paclitaxel (Tax), or 5 μM arsenite (As) were grown in 6 cm dishes for 15 h. Detached cells were collected and adhered to poly-D-lysine slides before fixation and staining with anti-γ-tubulin (AlexaFluor 488, green), anti-histone H3-S10-P (a mitotic marker, AlexaFluor 594, red), and DAPI (blue). Cells were analyzed and photographed via fluorescence microscopy. Representative examples of three independent experiments are shown. White bar represents 50 micrometers. **B.** A minimum of 200 mitotic cells per experiment were analyzed and each mitotic cell was scored for number of centrosomes. Data from three independent experiments were graphed as a stacked mean percentage ± SD. Statistically significant differences between treatments are labeled (*** = $p < 0.01$).

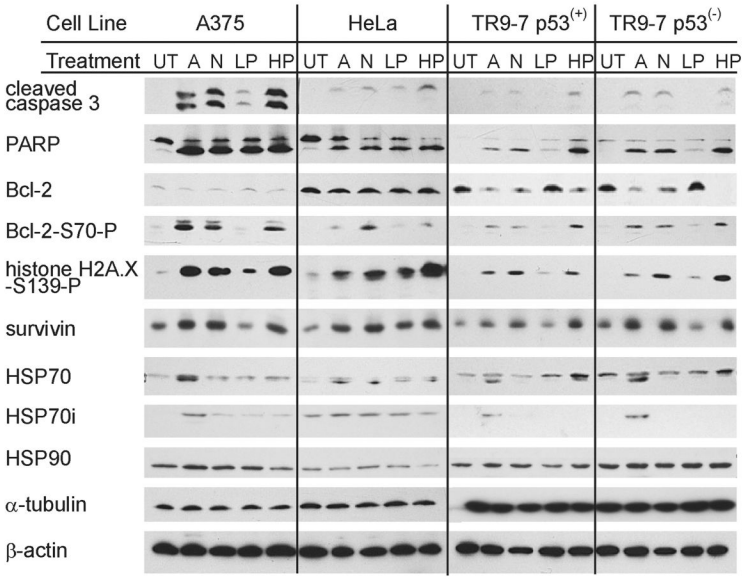

Figure 4. Western blot analysis of protein markers of mitotic arrest and apoptosis

A375, HeLa, TR9-7 p53$^{(+)}$, and TR9-7 p53$^{(-)}$ cells were untreated (UT), or treated with 5 μM arsenite (A), 90 ng/ml nocodazole (N), 7 nM paclitaxel (LP), or 100 nM paclitaxel (HP) for 24 h. Total cellular lysate proteins were resolved by SDS-PAGE, transferred to nitrocellulose membranes, and probed for cleaved caspase 3, PARP, Bcl-2, Bcl-2-S70-P, histone H2A.X-S139-P, survivin, HSP70, HSP70i, HSP90. α-tubulin and β-actin as indicated from top to bottom, respectively. Representative results of triplicate experiments are shown.

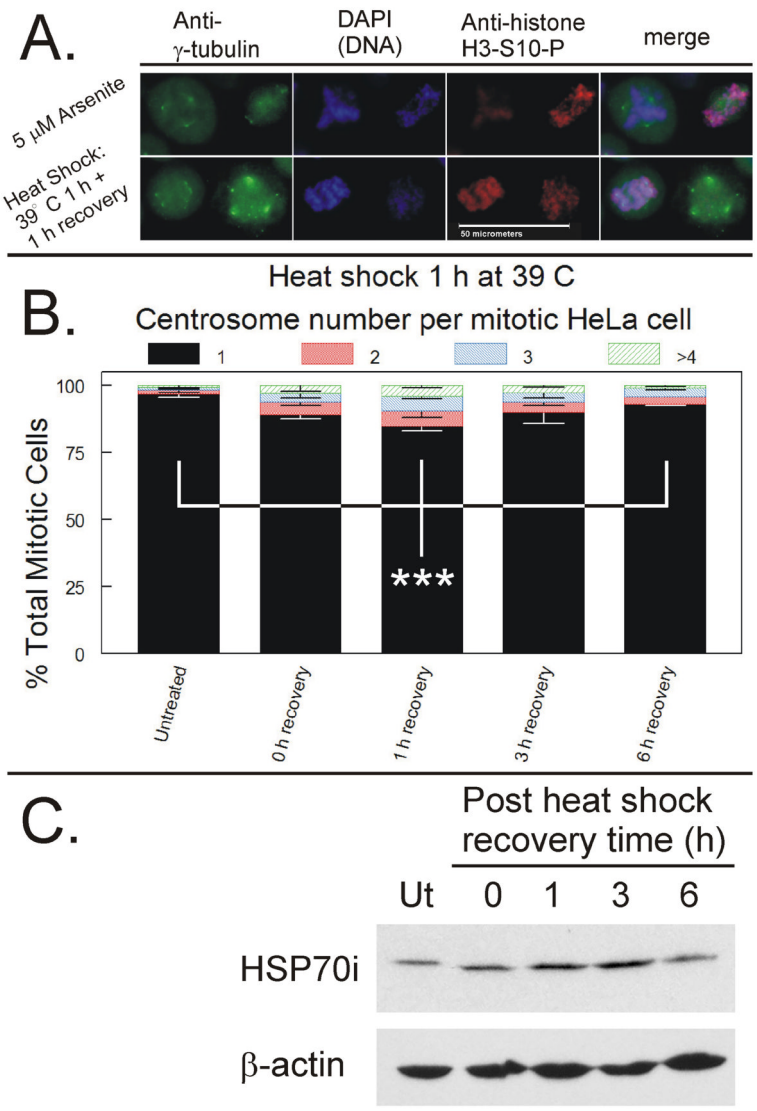

Figure 5. Immunofluorescence analysis of centrosomes in mitotic cells after heat shock

HeLa cells were subjected to heat shock by incubation for 1 h at 39° C. Mitotic cells were harvested at 0, 1, 3 and 6 h post-heat shock and analyzed by ICC for centrosome quantification. **A.** Representative examples of abnormal centrosome amplification induced by arsenite exposure or heat shock and allowed to recover for 1 h. White bar represents 50 micrometers. **B.** Quantification of centrosome number per mitotic cell. A minimum of 200 mitotic cells per experiment were analyzed and each mitotic cell was scored for number of centrosomes. Data from three independent experiments were graphed as a stacked mean percentage ± SD. Statistically significant differences between cells with one hour recovery and either untreated or cell after 6 h recovery (*** = $p < 0.01$). **C.** Cells were also collected for western blot analysis and total cellular lysate proteins were resolved by SDS-PAGE, transferred to nitrocellulose membranes, and probed for HSP70i and β-actin.

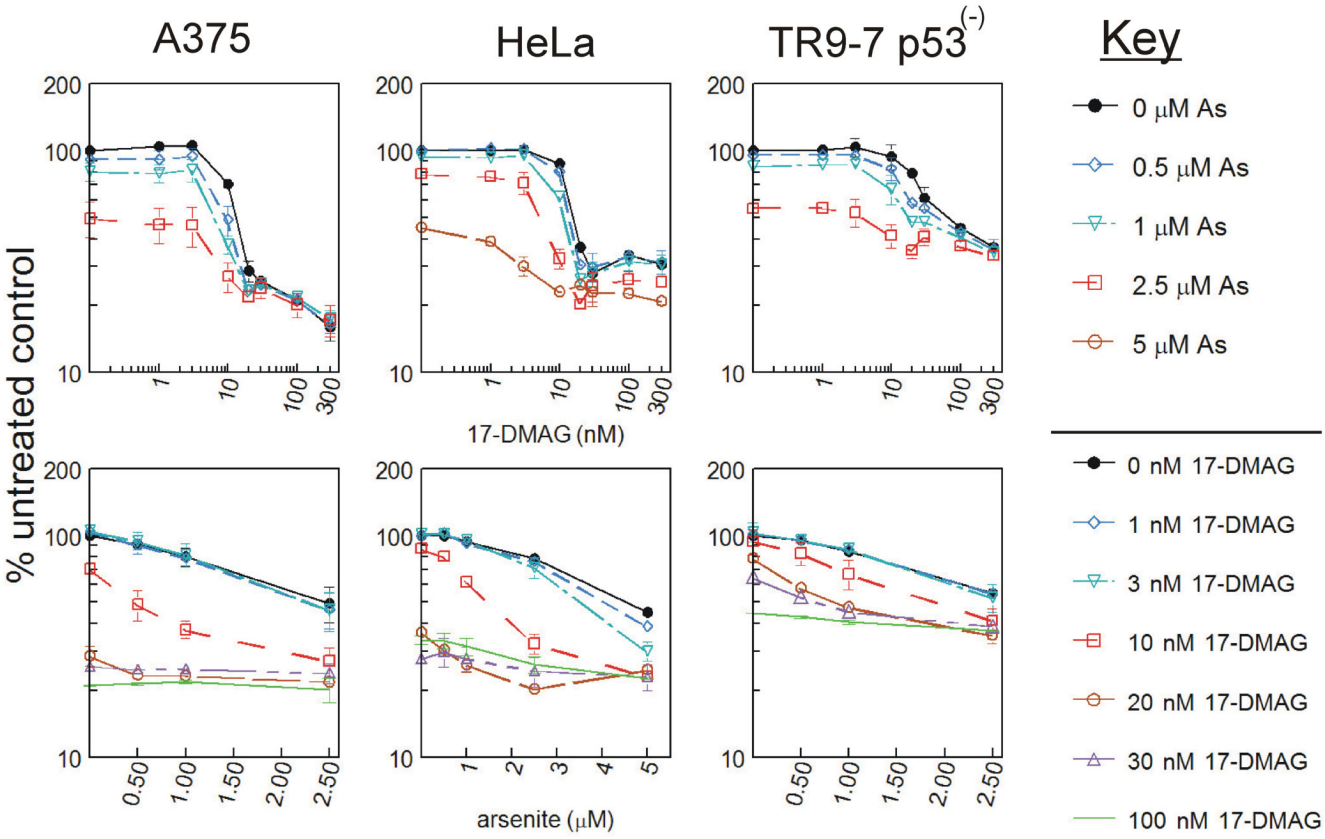

Figure 6. Cytotoxicity of HSP90 inhibitor 17-DMAG co-treatment with arsenite

A. A375, HeLa, and TR9-7 cells were plated on 96 well dishes in triplicate and exposed to 0-300 nM 17-DMAG in combination with 0, 0.5, 1, 2.5 or 5 μM arsenite for 48 h prior to analysis with AlamarBlue fluorescence assay. Data are graphed as mean ± SD from three independent experiments. Data are presented as percent untreated control either with 17-DMAG concentration on the X-axis (top graphs) or arsenite concentration on the X-axis (bottom graphs).

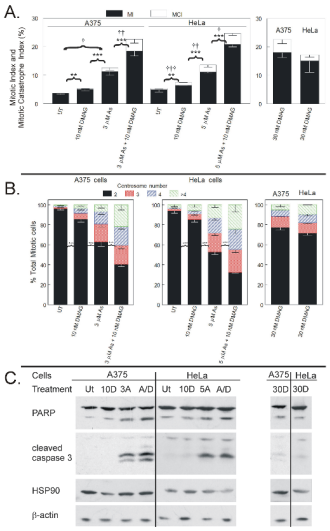

Figure 7. HSP90 inhibitor 17-DMAG enhances arsenite-induced mitotic arrest and centrosome abnormalities

A. A375 and HeLa cells were plated in 6 well dishes and treated with 0, 3 or 5 μM arsenite, 10 or 30 nM 17-DMAG, or 10 nM 17-DMAG in combination with 3 or 5 μM for 24 h before mitotic index analysis. Interphase nuclei, mitotic spreads and mitotic catastrophe were scored in 1,800 cells per condition. Statistically significant differences between mitotic index (MI) and mitotic catastrophe index (MCI) are labeled (MI: * = $p < 0.1$, ** = $p < 0.05$, *** = $p < 0.01$; MCI: † = $p < 0.1$, †† = $p < 0.05$, ††† = $p < 0.01$). **B**. HeLa and A375 cells were plated on 15 or 6 cm dishes exposed to 0, 3 or 5 μM arsenite, 10 or 30 nM 17-DMAG, or 10 nM 17-DMAG in combination with 3 or 5 μM for 15 h. Detached cells were collected and adhered to poly-D-lysine slides before fixation and staining with anti-γ-tubulin, anti-histone H3-S10-P, and DAPI. Centrosomes per mitotic cell were quantified. in a minimum of 200 mitotic cells per experiment. Data from three independent experiments are graphed as a stacked mean percentage ± SD. Statistically significant differences between treatments are labeled (* = $p < 0.1$, ** = $p < 0.05$, *** = $p < 0.01$). **C.** Total cellular lysate proteins of cells treated for 24 h were resolved by SDS-PAGE, transferred to nitrocellulose membranes, and probed for PARP, cleaved caspase 3, HSP90 and β-actin. Treatment conditions are: untreated (UT), 3 μM (A375, 3A) or 5 μM (HeLa, 5A) arsenite, 10 nM 17-DMAG (10D), 3 μM (for A375) or 5 μM (for HeLa) arsenite plus 10 nM 17-DMAG (A/D), and 30 nM 17-DMAG (30D).

Table 1

Arsenite and 17-DMAG interaction in cytotoxicity assay

IC50s were calculated from Figure 6 AlamarBlue viability assay data for A375, HeLa and TR9-7 p53$^{(-)}$ cells. Values for each line were calculated after normalizing data to both untreated control (top data set) as well as normalizing to respective arsenite treatment level for 17-DMAG IC50 calculations and to respective 17-DMAG treatment level for arsenite IC50 calculations (bottom data set). They were averaged and presented as concentration ± SD in the same organization as the graphs in Figure 6. Statistically significances differences between IC50 and value directly above it are labeled (* = $p < 0.1$, ** = $p < 0.05$, *** = $p < 0.01$).

IC50 values of cells treated with arsenite plus 17-DMAG

17-DMAG IC50 values (nM) ± STD normalized to untreated control			
As (μM)	A375	HeLa	TR9-7 p53$^{(-)}$
0	13.5 ± 0.6	16.0 ± 1.7	41.5 ± 6.5
0.5	10.6 ± 1.0***	14.2 ± 1.8	34.1 ± 5.8
1	8.9 ± 1.2*	11.7 ± 1.6**	24.9 ± 3.8**
2.5	3.3 ± 2.4***	5.8 ± 0.8***	5.4 ± 4.4
arsenite IC50 values (μM) ± STD normalized to untreated control			
17-DMAG (nM)	A375	HeLa	TR9-7 p53$^{(-)}$
0	3.3 ± 1.2	4.7 ± 0.2	2.8 ± 0.1
1	2.8 ± 0.8	4.3 ± 0.1**	2.8 ± 0.1
3	2.3 ± 0.5	3.8 ± 0.2**	2.6 ± 0.2
10	0.6 ± 0.2***	1.3 ± 0.4***	1.7 ± 0.2***
20	N/A	N/A	0.848 ± 0.004***
30	N/A	N/A	0.77± 0.08
17-DMAG IC50 values (nM) ± STD normalized to respective arsenite treatment			
As (μM)	A375	HeLa	TR9-7 p53$^{(-)}$
0	13.5 ± 0.6	16.0 ± 1.7	41.5 ± 6.5
0.5	11.1 ± 0.4***	15.3 ± 0.7	37.0 ± 5.4
1	10.5 ± 0.4**	12.8 ± 0.8**	35.9 ± 3.9**
2.5	9.9 ± 2.2	8.8 ± 0.9***	N/A
arsenite IC50 values (μM) ± STD normalized to respective 17-DMAG treatment			
17-DMAG (nM)	A375	HeLa	TR9-7 p53$^{(-)}$
0	3.3 ± 1.2	4.7 ± 0.2	2.8 ± 0.1
1	2.8 ± 0.8	4.3 ± 0.1**	2.8 ± 0.4
3	2.3 ± 0.5	3.8 ± 0.2***	2.7 ± 0.5
10	1.3 ± 0.4***	1.9 ± 0.1***	2.1 ± 0.4*
20	N/A	N/A	1.4 ± 0.2**
30	N/A	N/A	N/A